Electronic Supplementary Information

Acid and alkali-resistant Dy_4 coordination clusters: synthesis, structures and slow magnetic relaxation behaviors

Shui Yu,[a] Huancheng Hu,*[a] Yunkai Chen,[a] Zilu Chen,*[a] Zhanyun Zhang,[a] Man-Man Ding,[b] Yi-Quan Zhang,*[c] Dongcheng Liu,[a] Yuning Liang,[a] Fupei Liang*[a,c]

[a] State Key Laboratory for Chemistry and Molecular Engineering of Medicinal Resources, School of Chemistry and Pharmaceutical Sciences, Guangxi Normal University, Guilin 541004, P. R. China. E-mail: siniantongnian@126.com; zlchen@mailbox.gxnu.edu.cn; fliangoffice@yahoo.com

[b] Jiangsu Key Laboratory for NSLSCS, School of Physical Science and Technology, Nanjing Normal University, Nanjing 210023, P. R. China. E-mail: zhangyiquan@njnu.edu.cn

[c] Guangxi Key Laboratory of Electrochemical and Magnetochemical Functional Materials, College of Chemistry and Bioengineering, Guilin University of Technology, Guilin, 541004, P. R. China. E-mail: fliangoffice@yahoo.com
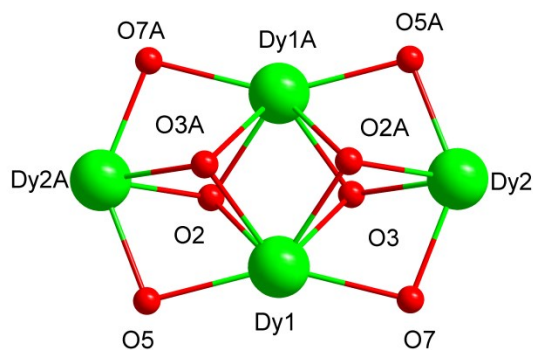
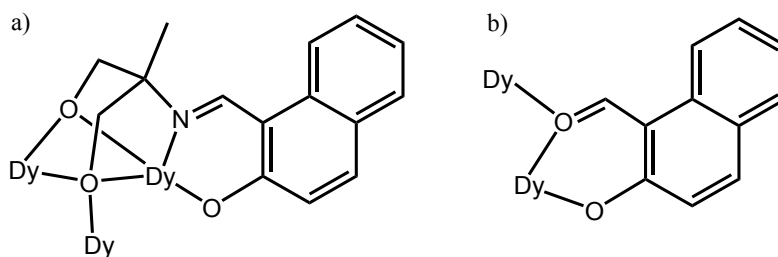**Fig. S1** The tetranuclear skeleton of **1**.

Fig. S2 Different bridging modes of (a) $(L^1)^{3-}$ and (b) $(L^2)^-$ in **1**.

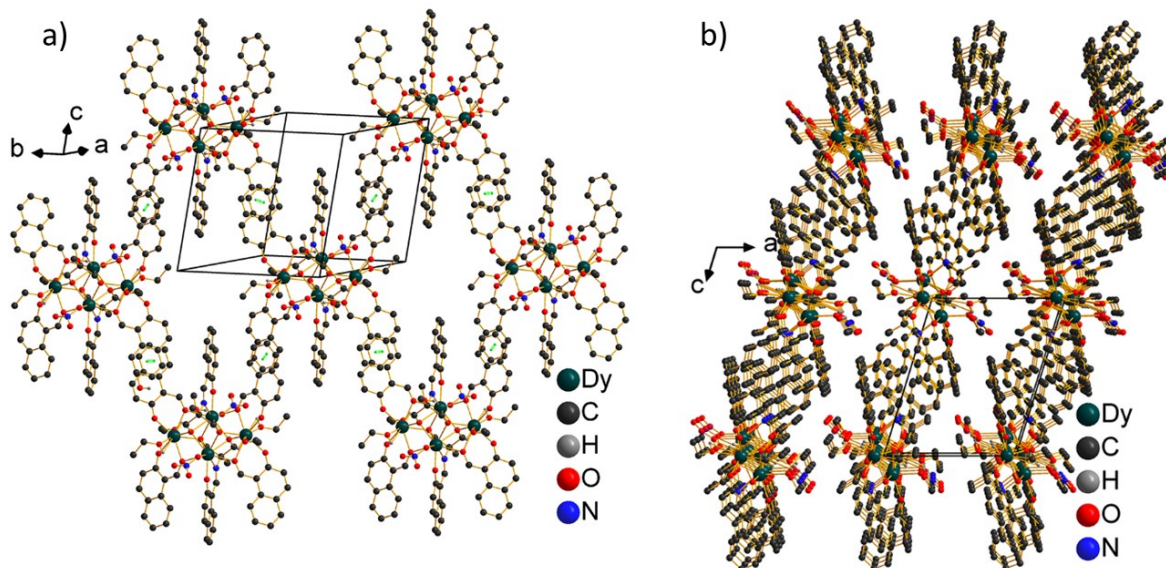**Fig. S3 (**a) A 2D supramolecular sheet in the $(\bar{1}\bar{1}1)$ plane of **1** formed via the connection of the tetranuclear units through π⋯π stacking interactions (green broken lines) along directions (101) and (011). (b) Packing diagram of **1**. The π⋯π stacking interactions along direction (101) are formed by parallel rings C30-C35 bearing symmetry codes (x, y, z) and (1- x, -y, 1- z) with an inter-plane distance of 3.3086(8) Å and a center-to-center distance of 3.8493(8) Å. The π⋯π stacking interactions along direction (011) are formed by parallel rings C19-C24 bearing symmetry codes (x, y, z) and (-x, 1 - y, 1 -

z) with an inter-plane distance of 3.5442(8) Å and a center-to-center distance of 3.8891(8) Å.
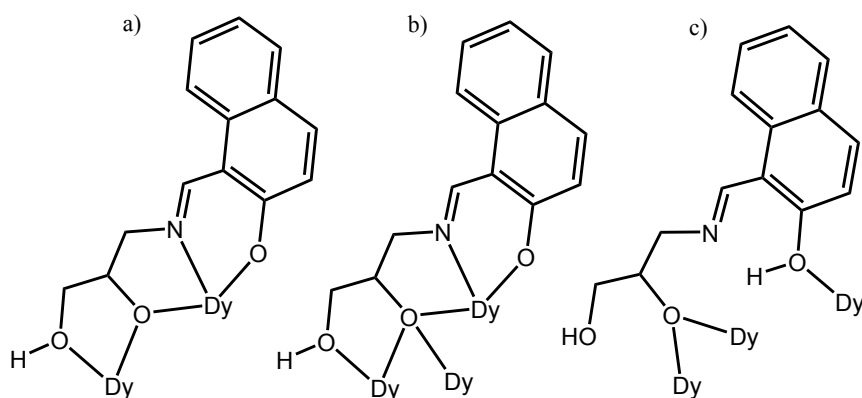
Fig. S4 Different bridging modes of (a and b) $(HL^3)^{2-}$ and (c) $(H_2L^3)^-$ in **2**.
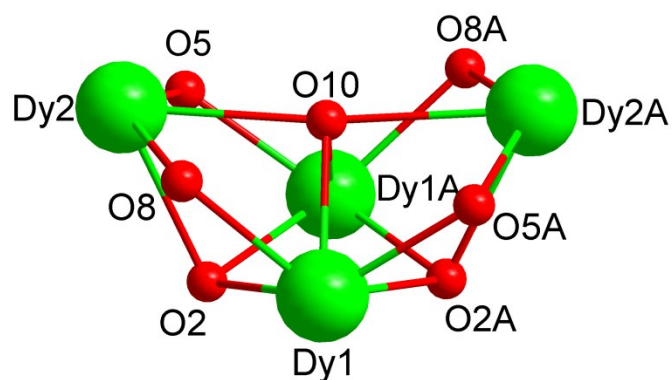
Fig. S5 The tetranuclear skeleton of **2**.
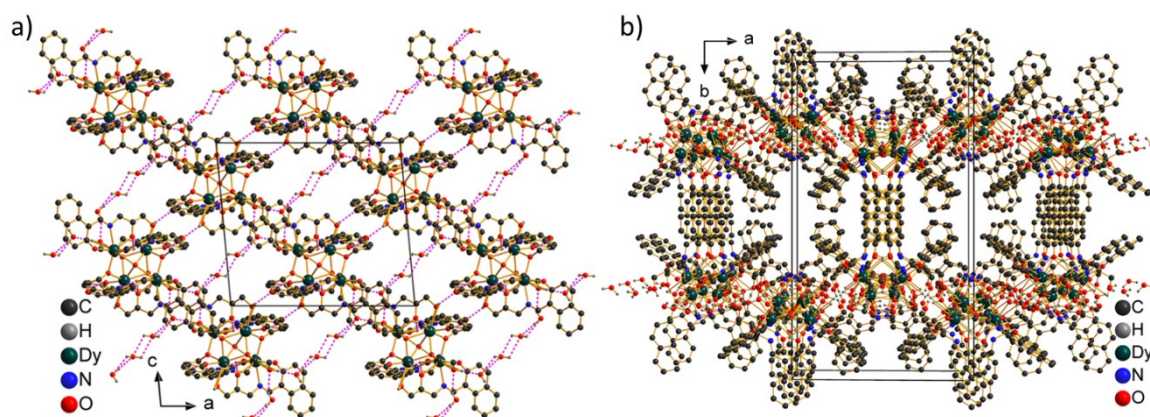
Fig. S6 (a) 2D supramolecular sheet of **2** via the connection of tetranuclear units by lattice water molecules through H-bonds. (b) The stacking diagram of the 2D supramolecular sheets of **2** along axis b. No significant π···π stacking interactions were found between the phenyl rings from the adjacent 2D supramolecular sheets.
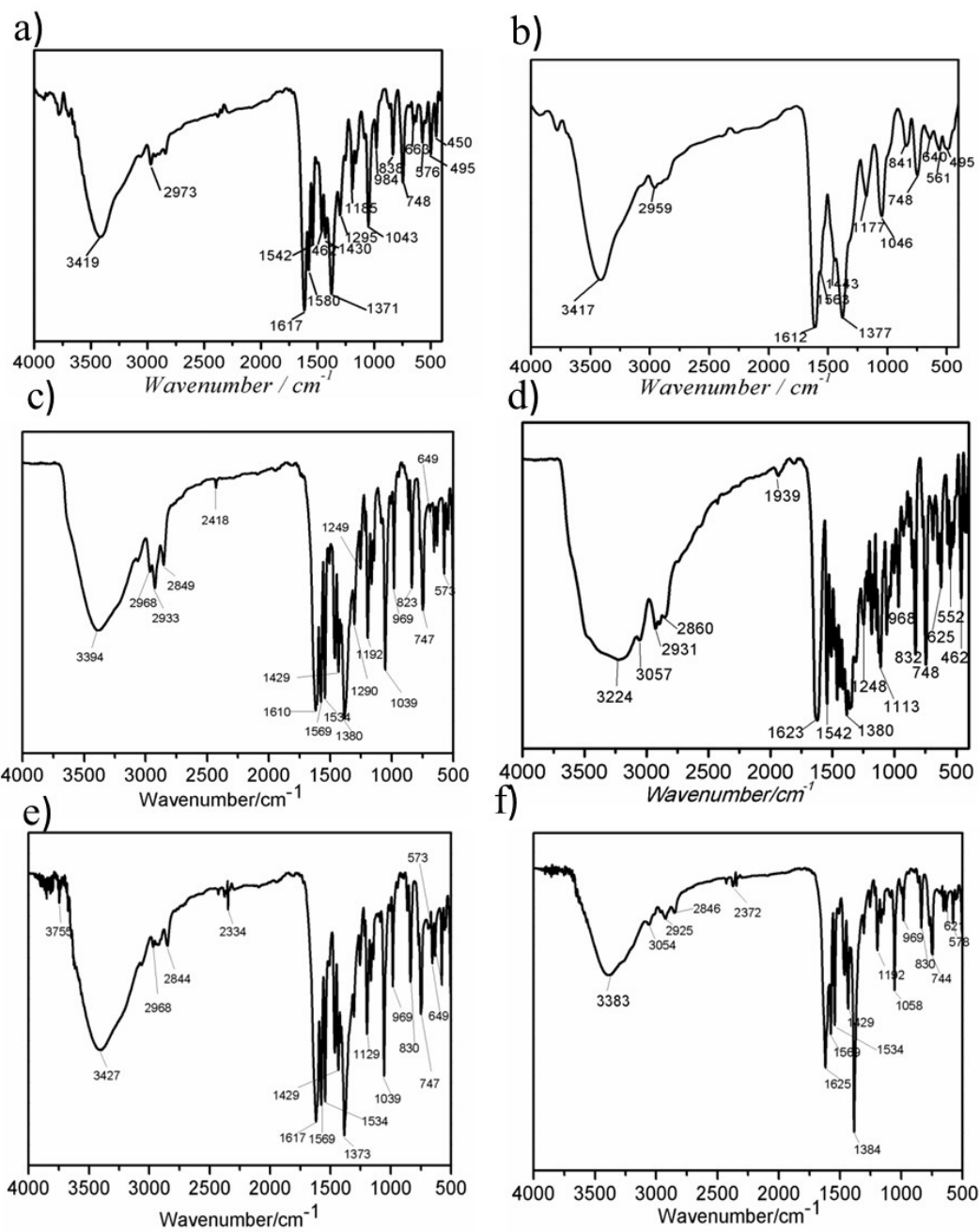
Fig. S7 FT-IR spectrum of (a) **1**, (b) **2**, (c) **1·Gd$_4$**, (d) **2·Gd$_4$**, (e) **1·Dy$_{0.42}$Y$_{3.58}$** and (f) **2·Dy$_{0.27}$Y$_{3.73}$**.
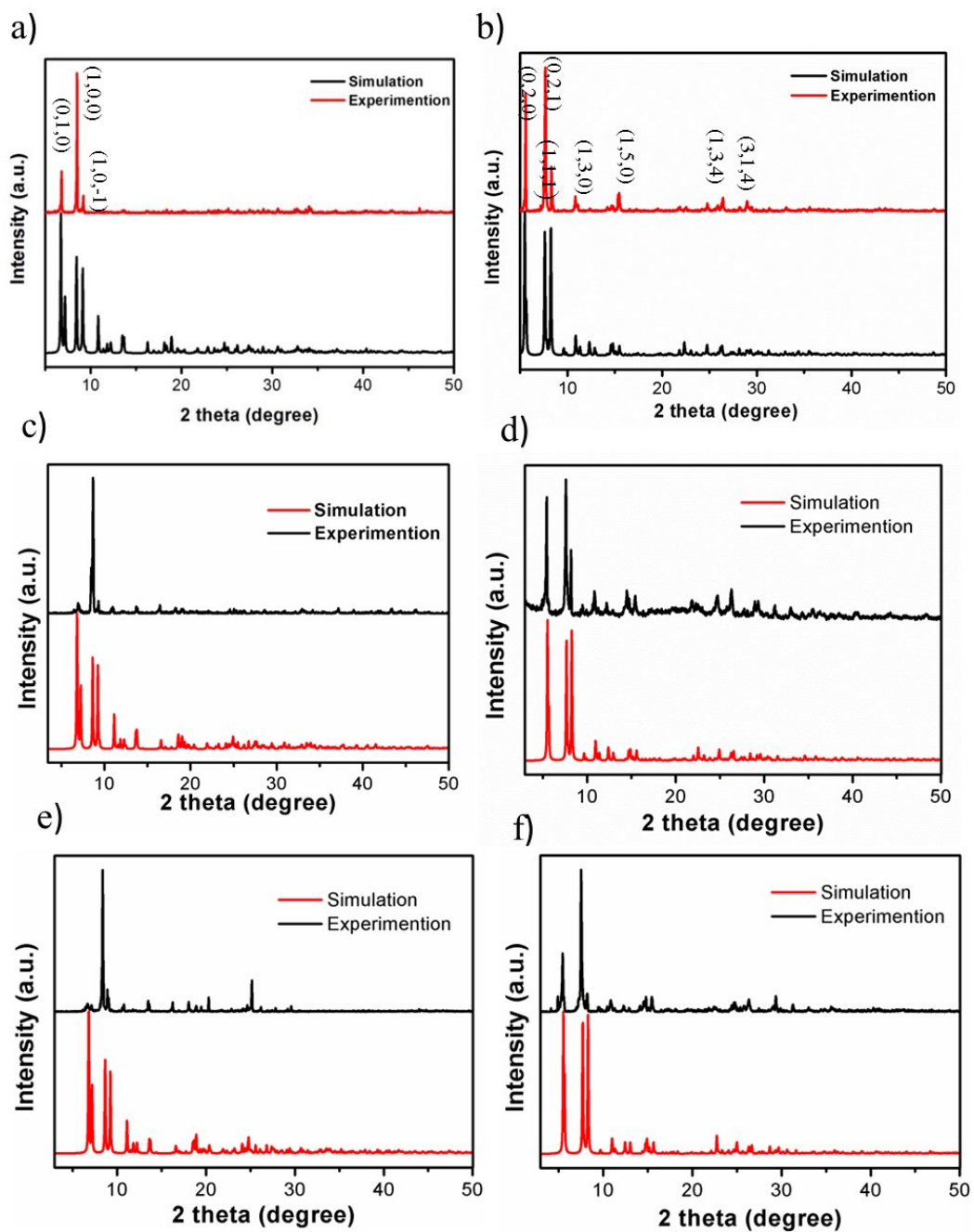
Fig. S8 The experimental and simulated PXRD patterns of (a) **1**, (b) **2**, (c) **1·Gd$_4$**, (d) **2·Gd$_4$**, (e)**1·Dy$_{0.42}$Y$_{3.58}$** and (f) **2·Dy$_{0.27}$Y$_{3.73}$**.
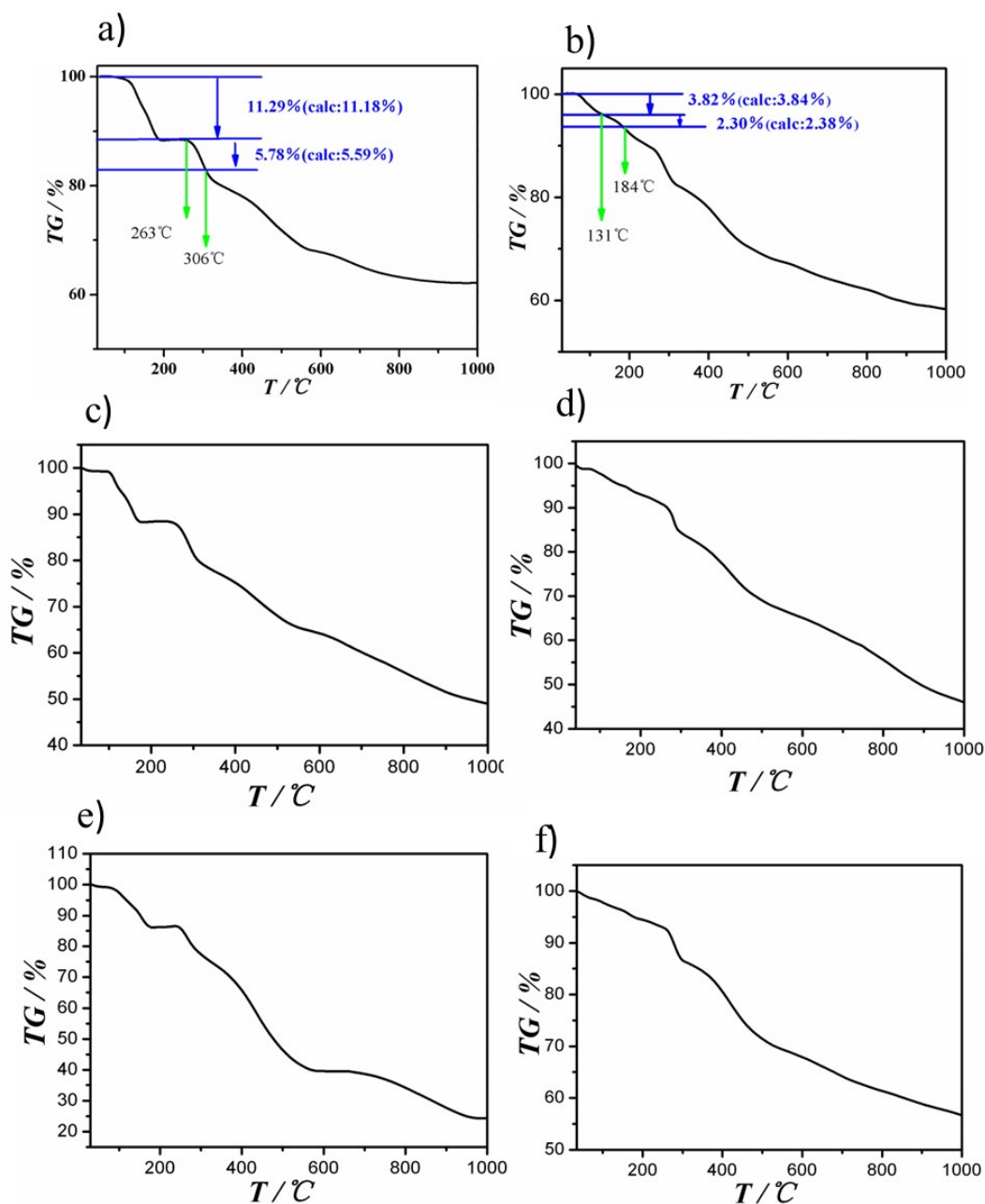
Fig. S9 The TGA curves of (a) **1**, (b) **2**, (c) **1·Gd$_4$**, (d) **2·Gd$_4$**, (e)**1·Dy$_{0.42}$Y$_{3.58}$** and (f) **2·Dy$_{0.27}$Y$_{3.73}$**.
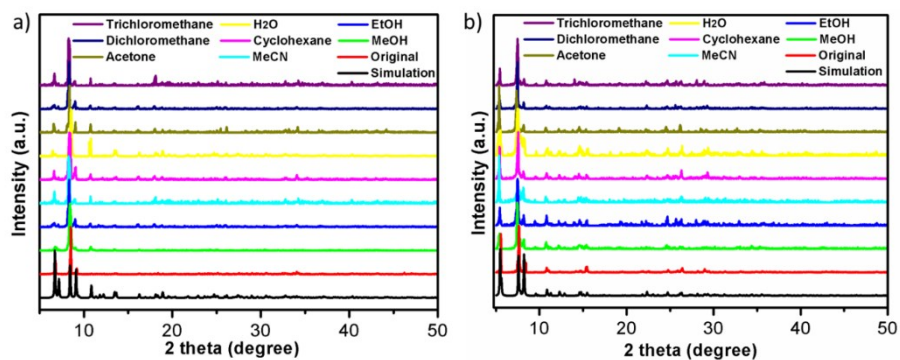
Fig. 10 The PXRD patterns of simulation, as-synthesized samples (a) **1** and (b) **2** after treated in

common solvents for 7 days at room temperature.
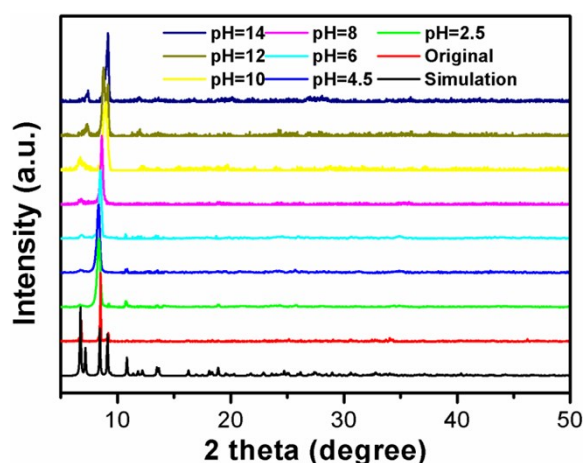
Fig. 11 The PXRD patterns of simulation, as-synthesized sample and the soaked sample of **1** in different pH values for two days.
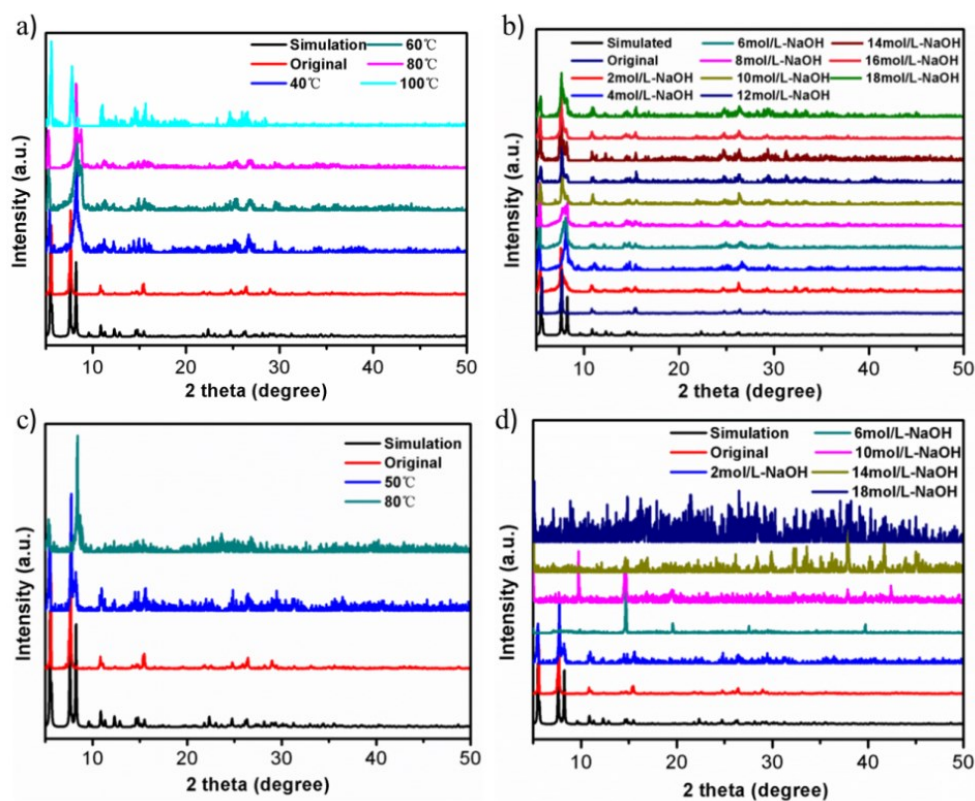
Fig. S12 The PXRD patterns of simulation, as-synthesized **2** and **2** soaked in (a) water at different temperatures for one day, (b) different concentrations of NaOH aqueous solutions for two days, (c) 2 M NaOH aqueous solution at 50 °C and 80 °C for one day, and (d) different concentrations of NaOH aqueous solutions at 50 °C for one day.
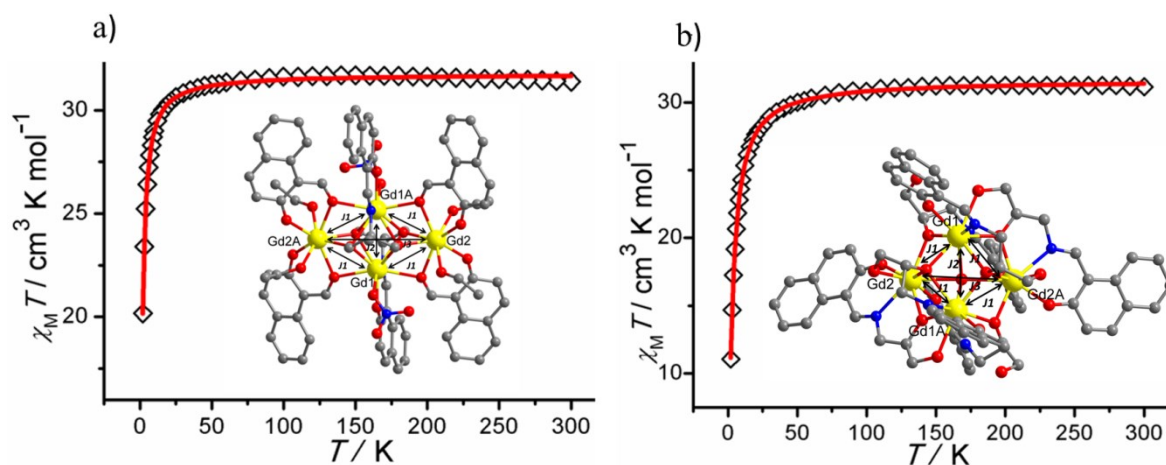
Fig. S13. $\chi_M T$ *vs.* T curves for (a) **1·Gd₄** and (b) **2·Gd₄** under an applied field of 1000 Oe (red solid lines represent the best fit using PHI program. Inset: Scheme of the Gd^{III}-Gd^{III} interactions in compounds **1·Gd₄** and **2·Gd₄**).
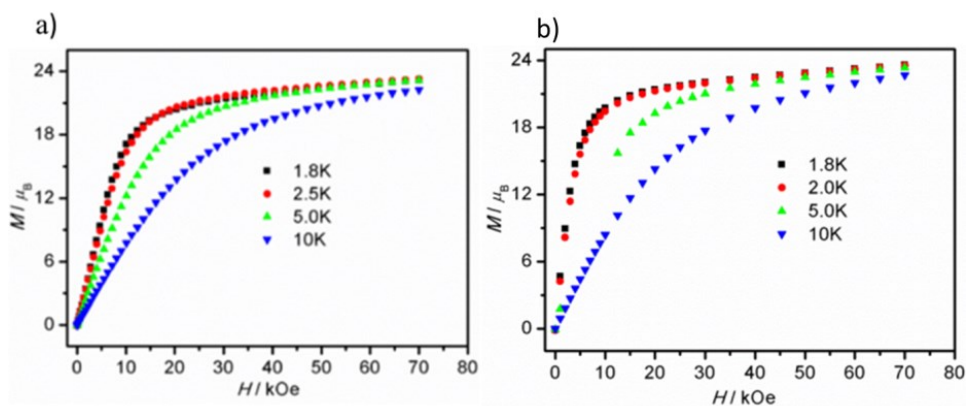
Fig. S14 M versus H plots for (a) **1** and (b) **2** at different temperatures.
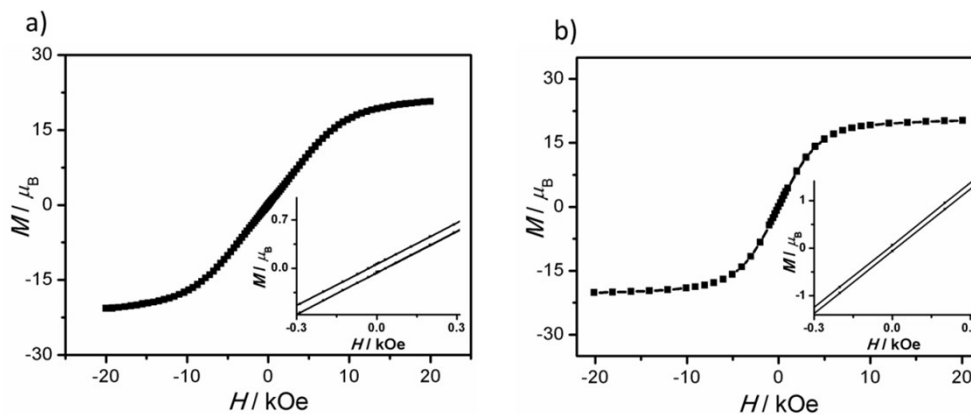
Fig. S15 Plots of magnetic hysteresis loops for (a) **1** and (b) **2**.
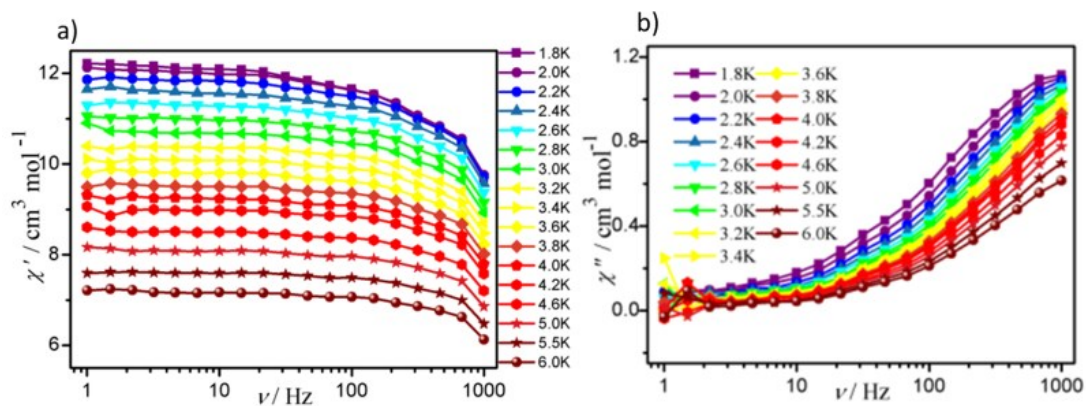
Fig. S16 Frequency-dependent (a) in-phase (χ') and (b) out-of-phase (χ'') ac susceptibilities under zero dc field for **1**.
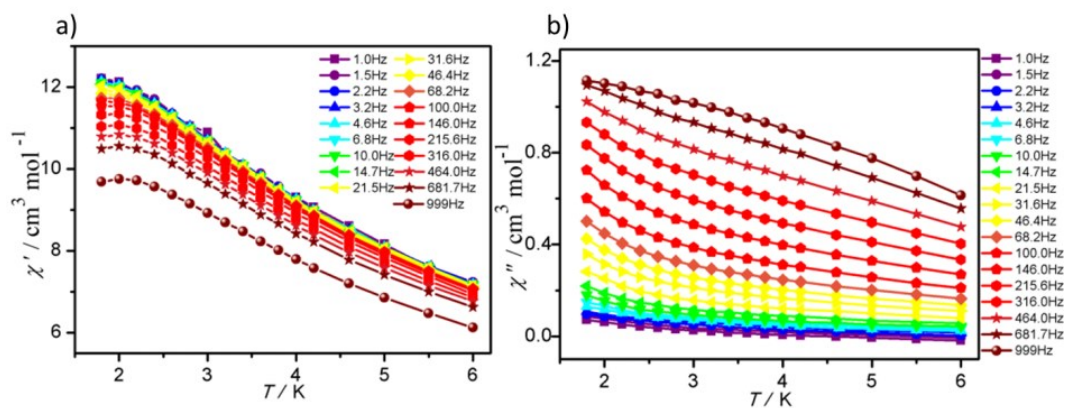
Fig. S17 Temperature-dependent (a) χ' and (b) χ'' ac susceptibilities under zero dc field for **1**.
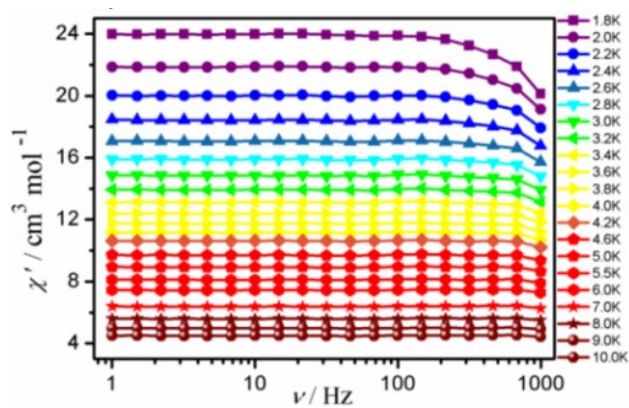
Fig. S18 Frequency-dependent χ' ac susceptibilities under zero dc field for **2**.
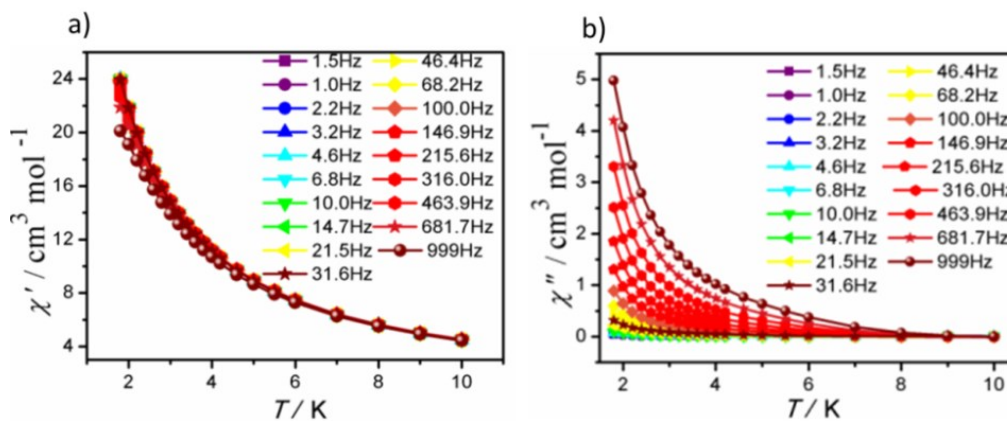
Fig. S19 Temperature-dependent (a) χ' and (b) χ'' ac susceptibilities under zero dc field for **2**.
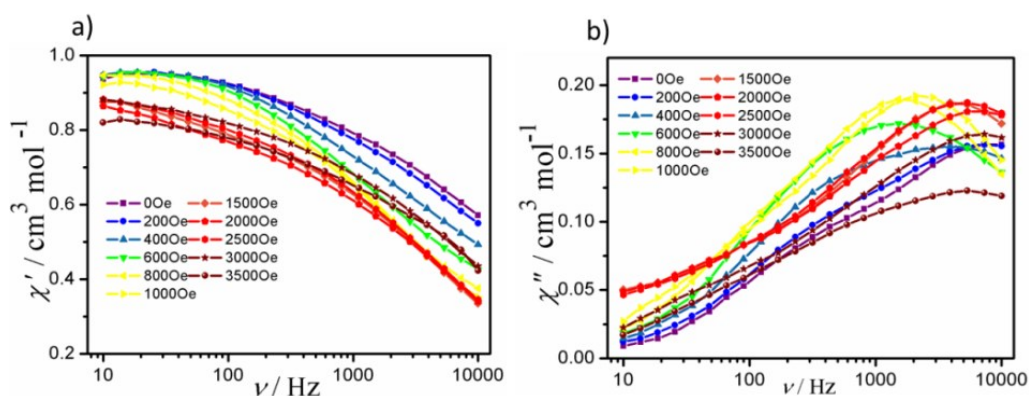
Fig. S20 Frequency-dependent (a) χ' and (b) χ'' ac susceptibilities under different dc fields for **1** at 2 K.
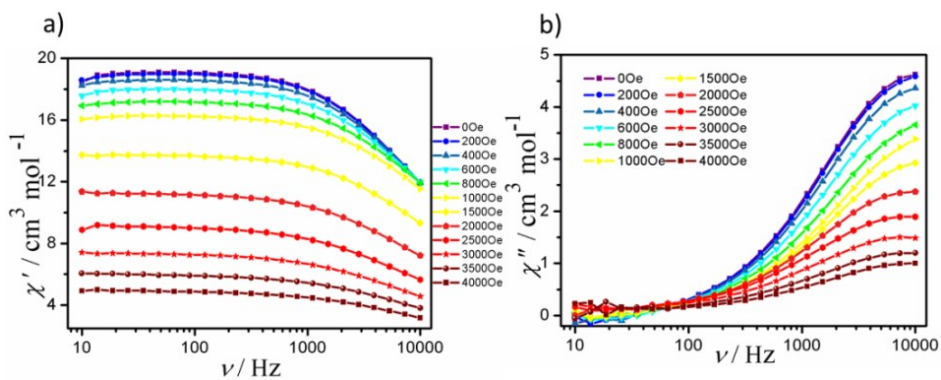
Fig. S21 Frequency-dependent (a) χ' and (b) χ'' ac susceptibilities under different dc fields for **2** at 2 K.
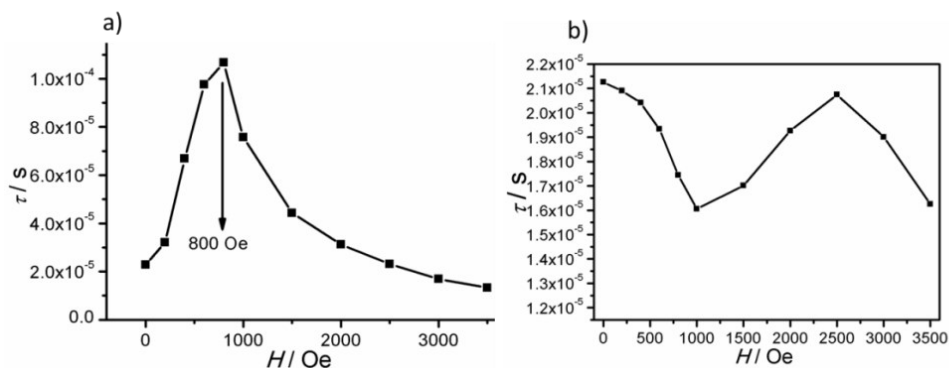
Fig. S22 Plots of the relaxation time τ vs. H for (a) **1** and (b) **2**.
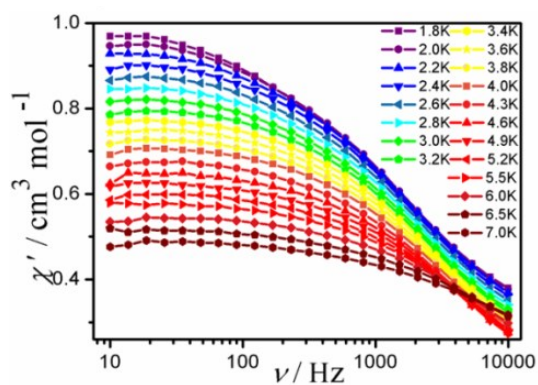
Fig. S23 Frequency-dependent χ' ac susceptibilities for **1** under 800 Oe.
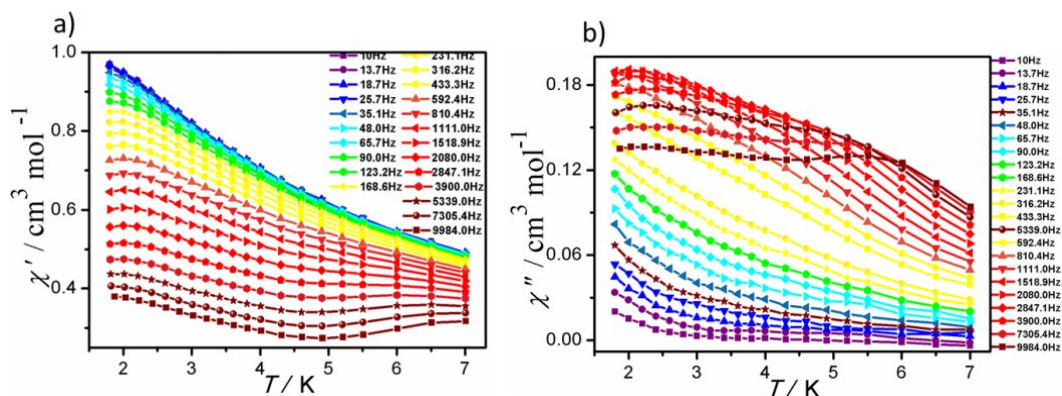
Fig. S24 Temperature-dependent (a) χ' and (b) χ'' ac susceptibilities for **1** under 800 Oe.
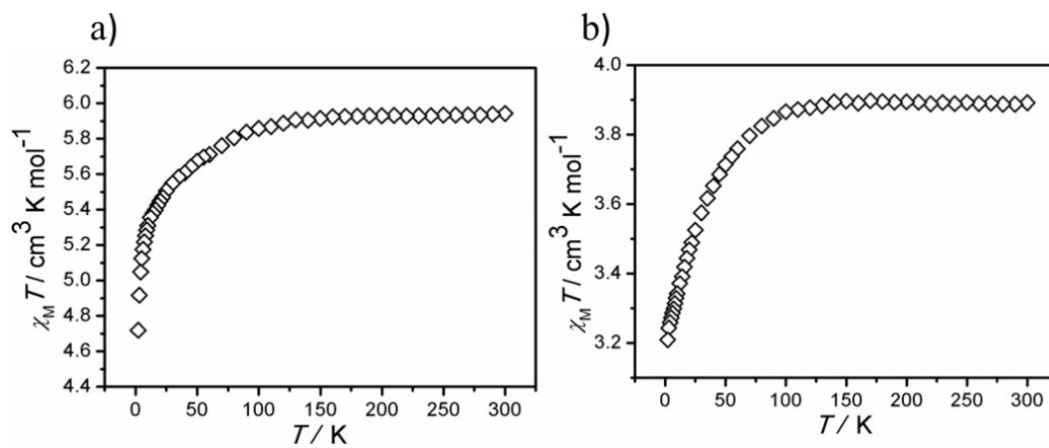
Fig. S25 $\chi_M T$ versus T curves for (a) **1·Dy$_{0.42}$Y$_{3.58}$** and (b) **2·Dy$_{0.27}$Y$_{3.73}$**.
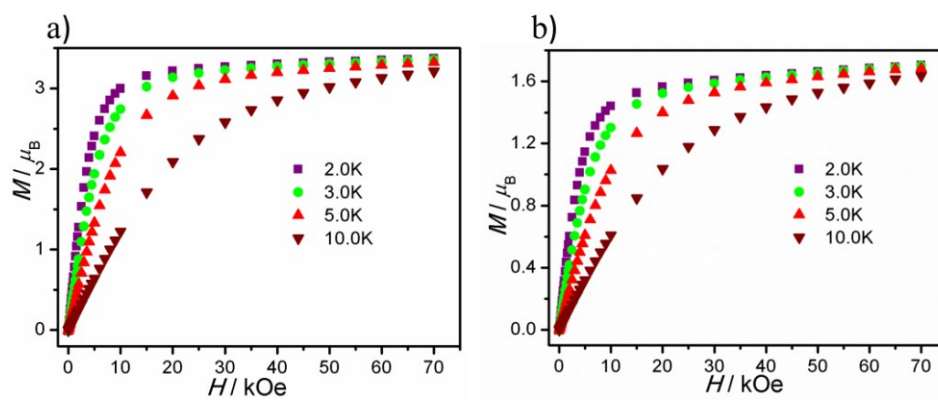
Fig. S26 M versus H curves for (a) **1·Dy$_{0.42}$Y$_{3.58}$** and (b) **2·Dy$_{0.27}$Y$_{3.73}$**.
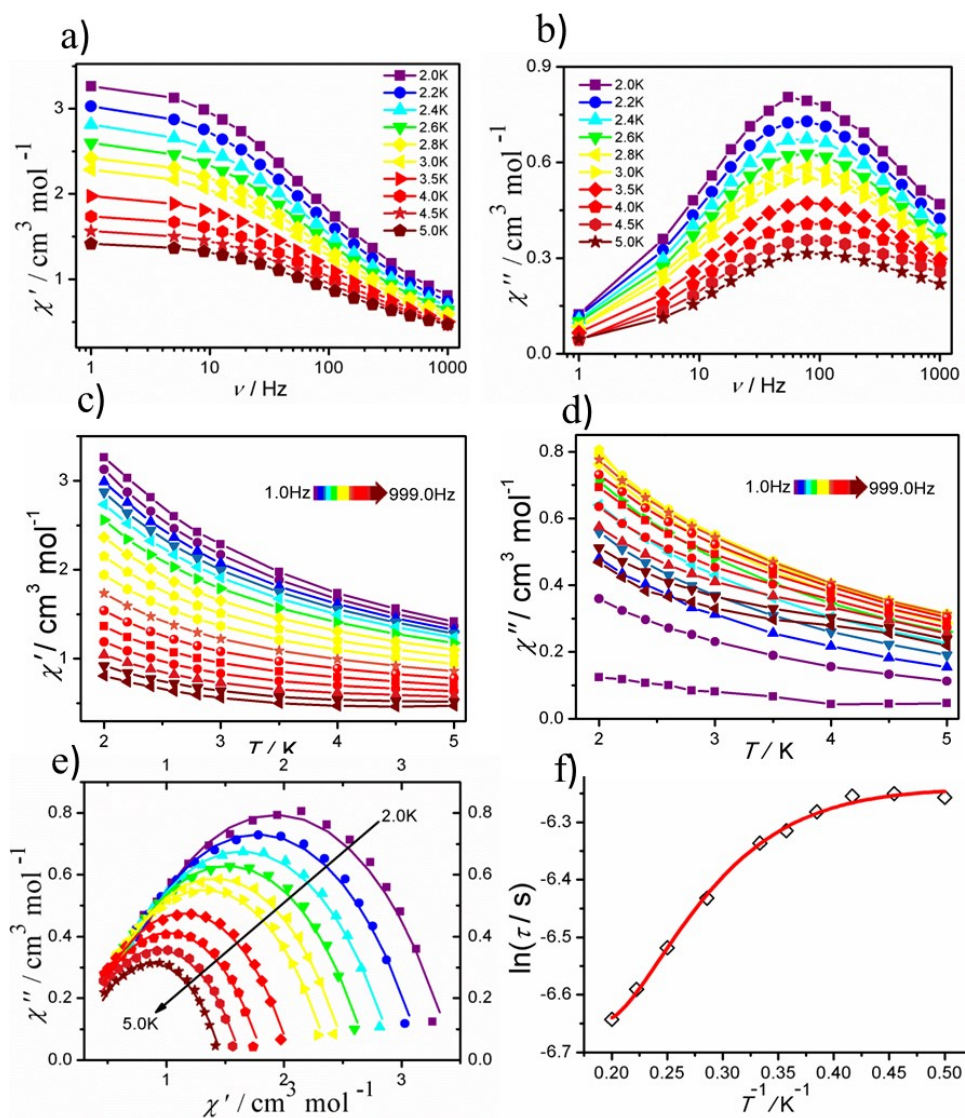
Fig. S27 Frequency-dependent (a) χ' and (b) χ'' ac susceptibilities, temperature-dependent (c) χ' and (d) χ'' ac susceptibilities, (e) Cole-Cole diagrams with the solid lines representing the best fit to the generalized Debye model and (f) plots of $\ln(\tau)$ vs. T^{-1} with solid lines representing the best simulation based on the multiple relaxation pathways for $\mathbf{1 \cdot Dy_{0.42}Y_{3.58}}$ under zero dc field.
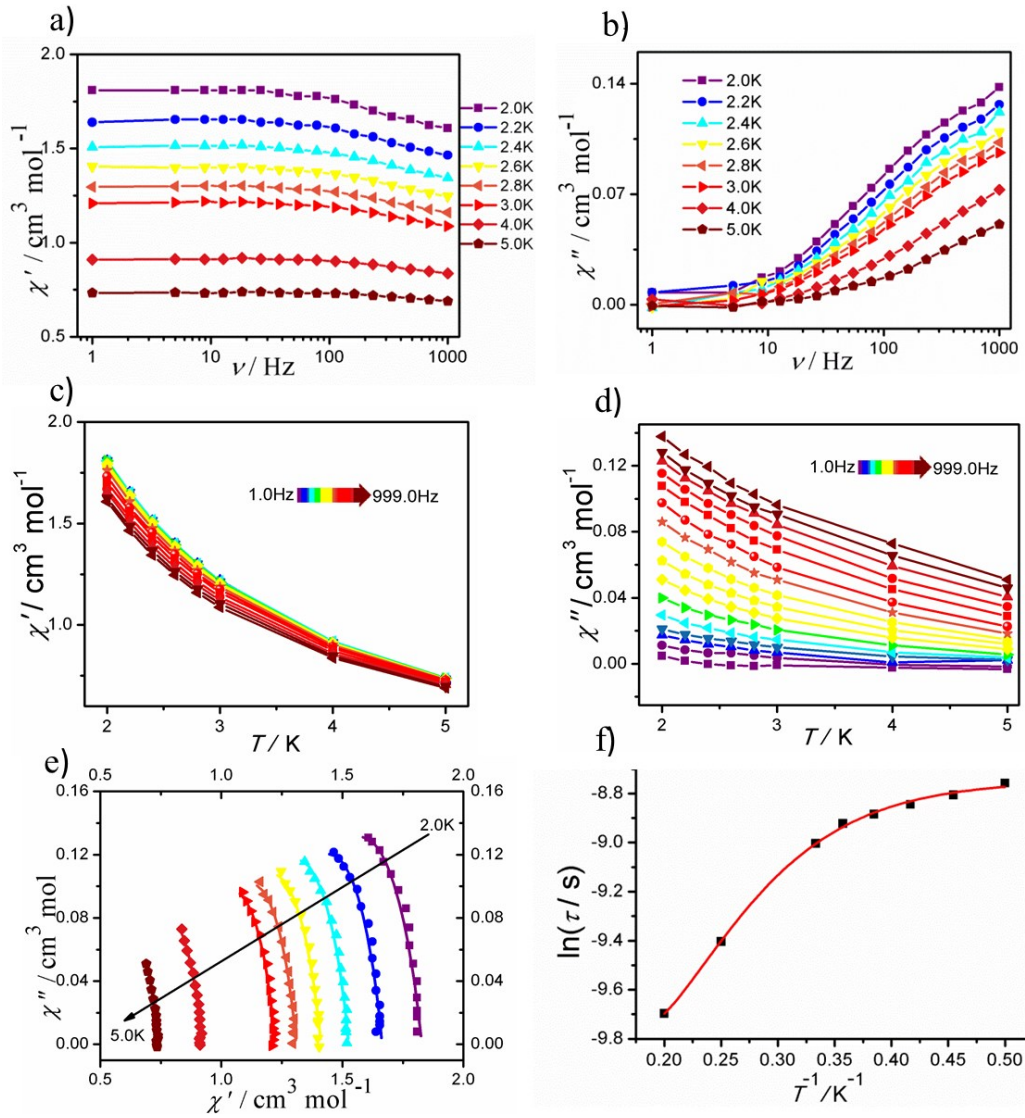
Fig. S28 Frequency-dependent (a) χ' and (b) χ'' ac susceptibilities, temperature-dependent (c) χ' and (d) χ'' ac susceptibilities, (e) Cole-Cole diagrams with the solid lines representing the best fit to the generalized Debye model and (f) plots of $\ln(\tau)$ vs. T^{-1} with solid lines representing the best simulation based on the multiple relaxation pathways for **2·Dy$_{0.27}$Y$_{3.73}$** under zero dc field.

Eqn S1 and S2 Equations for a generalized Debye model used for fitting Cole−Cole diagrams

$$\chi_{AC}(\omega) = \chi_s + \frac{\chi_T - \chi_s}{1 + (i\omega\tau)^{(1-\alpha)}}$$

Splitting the above equation into its real and imaginary parts, one obtains:

14

$$\chi^{'}(\omega) = \chi_s + \frac{(\chi_T - \chi_s)[1 + (\omega\tau)^{1-\alpha}\sin\frac{1}{2}\alpha\pi]}{1 + 2(\omega\tau)^{(1-\alpha)}\sin\frac{1}{2}\alpha\pi + (\omega\tau)^{2(1-\alpha)}} \quad (S1)$$

$$\chi^{''}(\omega) = \frac{(\chi_T - \chi_s)(\omega\tau)^{1-\alpha}\cos\frac{1}{2}\alpha\pi]}{1 + 2(\omega\tau)^{(1-\alpha)}\sin\frac{1}{2}\alpha\pi + (\omega\tau)^{2(1-\alpha)}} \quad (S2)$$

Table S1. Crystallographic data and structural refinement parameters for **1**, **2**, **1·Gd$_4$** and **2·Gd$_4$**.

compound	**1**	**2**	**1·Gd$_4$**	**2·Gd$_4$**
formula	$C_{84}H_{88}Dy_4N_4O_{26}$	$C_{88}H_{95}Dy_4N_7O_{23}$	$C_{86}H_{92}Gd_4N_4O_{26}$	$C_{88}H_{95}Gd_4N_7O_{23}$
fw	2219.58	2268.70	2226.63	2247.70
T/ K	296.15	296(2)	101.15	173(2)
λ / Å	0.71073	0.71073	0.71073	1.54184
crystal system	triclinic	monoclinic	triclinic	monoclinic
space group	$P\bar{1}$	$C2/c$	$P\bar{1}$	$C2/c$
a / Å	11.094 (3)	17.976(6)	10.89930(10)	18.1829(7)
b / Å	14.715 (3)	32.213(10)	14.5536(2)	31.9555(8)
c / Å	14.882 (3)	15.971(5)	14.7744(2)	15.8990(5)
α / °	112.836 (3)	90.00	112.7460(10)	90
β / °	102.378 (3)	95.254(5)	102.1520(10)	96.130(4)
γ / °	97.985 (3)	90.00	99.4760(10)	90
V / Å^3	2119.4 (8)	9209(5)	2032.69(5)	9185.2(5)
Z	1	4	1	4
D_c / g·cm^{-3}	1.739	1.635	1.819	1.625
μ / mm^{-1}	3.564	3.282	3.304	18.995
2θ / °	3.1 to 50.02	3.502 to 50.038	3.134 to 50.018	5.532 to 157.884
$F(000)$	1092.0	4480.0	1100.0	4448.0
reflns collected	22506	36712	40949	32943

reflns unique	7471	8011	7162	9330
R_{int}	0.0337	0.0623	0.0362	0.0534
GOF on F^2	1.108	1.074	1.037	1.030
R_1 (I > 2σ(I))	0.0372	0.0381	0.0241	0.0730
ωR_2 (I > 2σ(I))	0.0879	0.0920	0.0554	0.2058
R_1 (all data)	0.0471	0.0645	0.0281	0.0883
ωR_2 (all data)	0.0974	0.1097	0.0574	0.2216

Table S2. Selected bond lengths / Å and bond angles / ° for **1.**

Dy1-O7	2.499 (4)	O4A-Dy2-O3	144.24 (16)	O4A-Dy2-O2A	108.30 (17)
Dy1-O3	2.565 (4)	O4A-Dy2-O5A	71.57 (16)	O2-Dy1-O7	125.81 (14)
Dy1-O3A	2.404 (4)	O3A-Dy1-O7	138.38 (14)	O2A-Dy1-O7	71.97 (14)
Dy1-O5	2.512 (4)	O3A-Dy1-O3	94.47 (13)	O2A-Dy1-O3	58.94 (13)
Dy1-N1	2.425 (5)	O3A-Dy1-O5	70.35 (14)	O2-Dy1-O3	62.84 (13)
Dy1-O8	2.431 (5)	O3A-Dy1-N1	129.69(15)	O2A-Dy1-O5	136.80 (14)
Dy1-O2A	2.406 (4)	O3A-Dy1-O8	78.55(15)	O2-Dy1-O5	66.03 (14)
Dy1-O2	2.490 (4)	O3A-Dy1-O2A	66.47(14)	O2A-Dy1-N1	127.15 (15)
Dy1-O1	2.230 (4)	O3A-Dy1-O2	60.04 (13)	O2A-Dy1-O8	80.34 (16)

Dy2-O6	2.248 (5)	O5-Dy1-O3	127.20(14)	O2A-Dy1-O2	92.82 (13)
Dy2-O7	2.404 (4)	N1-Dy1-O7	78.52 (15)	O1-Dy1-O7	78.77 (15)
Dy2-O3	2.331 (4)	N1-Dy1-O3	69.10 (15)	O1-Dy1-O3	131.15 (14)
Dy2-O5A	2.426 (4)	N1-Dy1-O5	82.54 (16)	O1-Dy1-O3A	133.73 (15)
Dy2-O11	2.430 (5)	N1-Dy1-O8	144.67 (16)	O1-Dy1-O5	74.73 (15)
Dy2-O12	2.414 (6)	N1-Dy1-O2	70.45 (14)	O1-Dy1-N1	72.59 (16)
Dy2-O2A	2.331 (4)	O8-Dy1-O7	92.66 (16)	O1-Dy1-O8	72.14 (16)
Dy2-O4A	2.254 (5)	O8-Dy1-O3	137.46 (16)	O1-Dy1-O2	128.47 (14)
Dy1···Dy1A	3.5877(10)	O8-Dy1-O5	90.23 (17)	O1-Dy1-O2A	138.47 (15)
Dy1···Dy2	3.5859(9)	O8-Dy1-O2	136.85 (15)	O7-Dy1-O5	151.03 (14)
Dy2···Dy2A	5.0410(10)	O7-Dy1-O3	64.98 (14)	O3-Dy2-O7	70.13 (14)
O6-Dy2-O7	71.80 (16)	O7-Dy2-O5A	137.45 (14)	O3-Dy2-O5A	73.08 (14)
O6-Dy2-O3	114.46 (17)	O7-Dy2-O11	70.41 (16)	O3-Dy2-O11	129.03 (16)
O6-Dy2-O5A	145.34 (17)	O7-Dy2-O12	118.31 (18)	O3-Dy2-O12	79.66 (17)
O6-Dy2-O11	81.6 (2)	O5A-Dy2-O11	121.36(17)	O3-Dy2-O2A	63.38 (14)
O6-Dy2-O12	74.26 (19)	O12-Dy2-O5A	74.16 (18)	O2A-Dy2-O7	74.98 (14)
O6-Dy2-O2A	144.65 (16)	O12-Dy2-O11	148.92 (19)	O2A-Dy2-O5A	69.87 (15)
O6-Dy2-O4A	92.19 (19)	O4A-Dy2-O11	75.87 (18)	O2A-Dy2-O11	76.20 (17)
O4A-Dy2-O7	144.28 (16)	O4A-Dy2-O12	85.7 (2)	O2A-Dy2-O12	134.10 (16)

Symmetry codes: (A) −x, −y, −z.

Table S3. Selected bond lengths / Å and bond angles / ° for **2**.

Dy1-O5A	2.254 (4)	O5A-Dy1-N1A	96.82 (18)	O5-Dy2-O3	94.73 (18)
Dy1-O1A	2.266 (4)	O1A-Dy1-N1A	72.64 (17)	O7A-Dy2-O3	160.15 (18)
Dy1-O8	2.336 (4)	O8-Dy1-N1A	157.06 (17)	O8-Dy2-O3	97.36 (18)

Dy1-O2	2.342 (4)	O2-Dy1-N1A	99.35 (18)	O4-Dy2-O2	139.86 (17)
Dy1-O10	2.446 (4)	O10-Dy1-N1A	129.52 (16)	O5-Dy2-O2	72.99 (15)
Dy1-N1A	2.471 (5)	O5A-Dy1-O2A	73.17 (14)	O7A-Dy2-O2	128.49 (16)
Dy1-O2A	2.472 (4)	O1A-Dy1-O2A	131.30 (15)	O8-Dy2-O2	75.24 (13)
Dy1-O6A	2.484 (5)	O8-Dy1-O2A	132.17 (14)	O3-Dy2-O2	66.24 (15)
Dy2-O4	2.225 (5)	O2-Dy1-O2A	75.75 (16)	O4-Dy2-N2	71.02 (18)
Dy2-O5	2.263 (4)	O5A-Dy1-N1A	96.82 (18)	O5-Dy2-N2	68.05 (17)
Dy2-O7A	2.329 (5)	O1A-Dy1-N1A	72.64 (17)	O7A-Dy2-N2	83.5 (2)
Dy2-O8	2.331 (4)	O8-Dy1-N1A	157.06 (17)	O8-Dy2-N2	154.27 (17)
Dy2-O3	2.410 (5)	O2-Dy1-N1A	99.35 (18)	O3-Dy2-N2	76.7 (2)
Dy2-O2	2.474 (4)	O10-Dy1-N1A	129.52 (16)	O2-Dy2-N2	122.65 (18)
Dy2-N2	2.510 (6)	O5A-Dy1-O2A	73.17 (14)	O4-Dy2-O10	139.36 (17)
Dy2-O10	2.5255 (7)	O1A-Dy1-O2A	131.30 (15)	O5-Dy2-O10	71.69 (12)
Dy1···Dy1A	3.6811 (10)	O8-Dy1-O2A	132.17 (14)	O7A-Dy2-O10	68.82 (17)
Dy1···Dy2	3.5859 (9)	O2-Dy1-O2A	75.75 (16)	O8-Dy2-O10	68.85 (11)
Dy2···Dy2A	5.0410(10)	O4-Dy2-O5	138.25 (16)	O3-Dy2-O10	127.72 (17)
O1A-Dy1-O2	85.14 (15)	O4-Dy2-O7A	88.02 (18)	O2-Dy2-O10	61.50 (15)
O8-Dy1-O2	77.73 (14)	O5-Dy2-O7A	79.65 (17)	N2-Dy2-O10	134.39 (14)
O5A-Dy1-O10	73.36 (12)	O4-Dy2-O8	83.51 (16)	O2-Dy1-O10	64.50 (12)
O1A-Dy1-O10	143.44 (12)	O5-Dy2-O8	137.67 (15)	O4-Dy2-O3	83.60 (19)
O8-Dy1-O10	70.16 (12)	O7A-Dy2-O8	99.54 (16)		

Symmetry codes: (A) −x+1, y, −z+1/2.

Table S4. Selected bond lengths / Å and bond angles / ° for **1·Gd₄**.

Gd1-O1	2.227 (2)	O1-Gd1-N1	72.56 (9)	O2A-Gd1-N1	127.07 (9)
Gd1-N1	2.420 (3)	O1-Gd1-O2A	138.24 (8)	O2A-Gd1-O2	92.59 (7)
Gd1-O2A	2.392 (2)	O1-Gd1-O2	128.91 (8)	O2-Gd1-O3	62.61 (7)
Gd1-O2	2.474 (2)	O1-Gd1-O3A	133.23 (8)	O2A-Gd1-O3	58.71 (7)
Gd1-O3A	2.384 (2)	O1-Gd1-O3	131.32 (8)	O2-Gd1-O5A	65.33 (8)
Gd1-O3	2.584 (2)	O1-Gd1-O5A	75.10 (8)	O2A-Gd1-O5A	137.46 (8)
Gd1-O5A	2.516 (2)	O1-Gd1-O7	78.59 (8)	O2A-Gd1-O7	72.13 (8)
Gd1-O7	2.491 (2)	O1-Gd1-O8	72.37 (8)	O2-Gd1-O7	125.37 (8)
Gd1-O8	2.431 (2)	N1-Gd1-O2	70.78 (9)	O2A-Gd1-O8	80.09 (8)
Gd2-O2A	2.331 (2)	N1-Gd1-O3	69.32 (8)	O3A-Gd1-N1	130.25 (9)
Gd2-O3	2.325 (2)	N1-Gd1-O5A	81.39 (9)	O3A-Gd1-O2	60.40 (8)
Gd2-O4	2.240 (2)	N1-Gd1-O7	77.91 (9)	O3A-Gd1-O2A	66.82 (8)
Gd2-O5	2.412 (2)	N1-Gd1-O8	144.86 (9)	O3A-Gd1-O3	94.89 (7)
Gd2-O6	2.249 (2)	O5A-Gd1-O3	126.03 (8)	O3A-Gd1-O5A	70.64 (8)
Gd2-O7	2.400 (2)	O7-Gd1-O3	64.87 (8)	O3A-Gd1-O7	138.88 (8)
Gd2-O12	2.401 (3)	O7-Gd1-O5A	150.37 (7)	O3A-Gd1-O8	77.76 (8)
Gd2-O11	2.425 (2)	O2A-Gd2-O5	69.17 (8)	O3-Gd2-O2A	63.37 (8)
O8-Gd1-O2	136.64 (8)	O2A-Gd2-O7	74.87 (8)	O3-Gd2-O5	73.48 (8)
O8-Gd1-O3	137.10 (8)	O2A-Gd2-O12	133.29 (9)	O3-Gd2-O7	70.37 (8)
O8-Gd1-O5A	91.71 (8)	O2A-Gd2-O11	75.37 (8)	O3-Gd2-O12	78.84 (9)
O8-Gd1-O7	93.13 (8)	O5-Gd2-O11	119.72 (8)	O3-Gd2-O11	128.48 (8)
O4-Gd2-O2A	108.47 (9)	O6-Gd2-O2A	145.15 (9)	O7-Gd2-O5	137.38 (8)
O4-Gd2-O3	144.75 (9)	O6-Gd2-O3	114.72 (9)	O7-Gd2-O12	118.39 (9)
O4-Gd2-O5	71.77 (8)	O6-Gd2-O5	145.61 (9)	O7-Gd2-O11	70.13 (8)
O4-Gd2-O6	91.39 (9)	O6-Gd2-O7	72.36 (8)	O12-Gd2-O5	74.71 (9)
O4-Gd2-O7	143.52 (9)	O6-Gd2-O12	74.51 (9)	O12-Gd2-O11	150.55 (9)
O4-Gd2-O12	86.48 (9)	O6-Gd2-O11	82.61 (9)	O4-Gd2-O11	75.63 (9)

Symmetry codes: (A) $-x$, $-y$, $-z$.

Table S5. Selected bond lengths / Å and bond angles / ° for **2·Gd₄**.

Gd1-O5A	2.283 (6)	O1A-Gd1-O2A	130.93 (19)	O4-Gd2-O5	137.3 (2)
Gd1-O1A	2.289 (6)	O8-Gd1-O2A	133.03 (18)	O4-Gd2-O7A	87.7 (3)
Gd1-O8	2.337 (6)	O2-Gd1-O2A	75.8 (3)	O5-Gd2-O7A	78.6 (2)
Gd1-O2	2.378 (6)	O10-Gd1-O2A	62.80 (15)	O4-Gd2-O8	84.3 (2)
Gd1-O10	2.445 (4)	O5A-Gd1-O6A	63.9 (2)	O5-Gd2-O8	137.6 (2)
Gd1-O2A	2.470 (6)	O1A-Gd1-O6A	75.7 (2)	O7A-Gd2-O8	100.0 (2)
Gd1-O6A	2.474 (6)	O8-Gd1-O6A	94.6 (2)	O4-Gd2-O3	85.5 (3)
Gd1-N1A	2.485 (7)	O2-Gd1-O6A	160.0 (2)	O5-Gd2-O3	93.5 (2)
Gd2-O4	2.252 (7)	O10-Gd1-O6A	131.1 (2)	O7A-Gd2-O3	159.5 (2)
Gd2-O5	2.282 (5)	O2A-Gd1-O6A	121.3 (2)	O8-Gd2-O3	98.5 (2)
Gd2-O7A	2.336 (6)	O5A-Gd1-N1A	98.4 (3)	O4-Gd2-O2	141.3 (2)
Gd2-O8	2.338 (5)	O1A-Gd1-N1A	71.6 (3)	O5-Gd2-O2	72.90 (19)
Gd2-O3	2.425 (7)	O8-Gd1-N1A	155.3 (2)	O7A-Gd2-O2	127.8 (2)
Gd2-O2	2.486 (6)	O2-Gd1-N1A	98.2 (2)	O8-Gd2-O2	75.47 (18)
Gd2-N2	2.529 (8)	O10-Gd1-N1A	129.6 (2)	O3-Gd2-O2	65.8 (2)
Gd2-O10	2.5538 (7)	O2A-Gd1-N1A	67.2 (2)	O4-Gd2-N2	70.5 (2)
O1A-Gd1-O2	85.1 (2)	O6A-Gd1-N1A	81.1 (3)	O5-Gd2-N2	68.0 (2)
O8-Gd1-O2	77.6 (2)	O8-Gd2-O10	68.94 (16)	O7A-Gd2-N2	83.7 (2)
O5A-Gd1-O10	73.40 (15)	O3-Gd2-O10	126.8 (2)	O8-Gd2-N2	154.4 (2)
O1A-Gd1-O10	143.21 (16)	O2-Gd2-O10	61.1 (2)	O3-Gd2-N2	75.8 (2)
O8-Gd1-O10	70.88 (15)	N2-Gd2-O10	134.5 (2)	O2-Gd2-N2	122.1 (2)
O2-Gd1-O10	64.13 (15)	O1A-Gd1-O2A	130.93 (19)	O4-Gd2-O10	139.6 (2)
O5A-Gd1-O2A	73.2 (2)	O7A-Gd2-O10	68.8 (2)	O5-Gd2-O10	71.34 (16)

Symmetry codes: (A) $-x+1$, y, $-z+1/2$

Table S6. ICP data of Dy(III) and Y(III) ions in **1·Dy₀.₄₂Y₃.₅₈** and **2·Dy₀.₂₇Y₃.₇₃**.

Compounds	Dy (μg / L)	Y (μg / L)	$C_{Dy:Y}$ (mol / L)
1·Dy₀.₄₂Y₃.₅₈	341.250	1591.417	0.42:3.58
2·Dy₀.₂₇Y₃.₇₃	219.375	1658.097	0.27:3.73

Table S7. The stability of some typical coordination compounds in different concentration of acid and/or alkali media.

Coordination Compounds	Dimension	Medium and Concentration	Temperature / °C	Time / h	Ref.
2	0 D	NaOH (2 M, 18 M)	50, RT	24, 48	This work
2	0 D	pH (2.5-14)	RT	168	This work
1	0 D	pH (2.5-14)	RT	168	This work
$Hf_{13}(\mu_4\text{-O})_8(OCH_3)_{36}$	0 D	HNO_3 (10 M), NaOH (20 M)	RT, 100	5, 2	1
$[Zn_5(H_2L^n)_6](NO_3)_4]\cdot 8H_2O\cdot 2CH_3OH$	0 D	HCl (12 M), $NH_3\cdot H_2O$ (14 M)	Refluxed	24	2
PTC-184-193	0 D	pH (1)	RT	168	3
PTC-184, -185, -188, -189, -190	0 D	pH (13)	RT	168	3
$TMA_8Ti_2Ta_8O_{28}\cdot 21H_2O$	0 D	pH (7.5-12)	NG	NG	4
$TMA_{10}Ti_{12}Ta_6O_{44}\cdot 39H_2O$	0 D	pH (7-11)	NG	NG	4
SLUG-34	1 D	pH (2, 4)	NG	12	5
$[Fe^{II}L(H_2O)]\cdot 2H_2O$	1 D	pH (1, 13)	NG	24	6
$[Eu_2(tpbpc)_4\cdot CO_3\cdot 4H_2O]\cdot DMF\cdot solvent$	1 D	pH (3-13)	NG	240	7
$\{[Tb(H_2O)(L)(TPA)]\cdot 0.5H_2O\}_n$	1 D	pH (2-12)	NG	24	8
$[Mg(ATDC)(H_2O)_2]_n$	2 D	pH (1-12)	RT	10	9
$\{Na[Zn_{1.5}(\mu_4\text{-O})(L)]\}_n$	2 D	pH (1-13)	NG	12	10
$[Cu_2I_2(BPEA)](DMF)_4$	2 D	pH (2-13)	NG	24	11
$\{[Ln_3(\mu_6\text{-CO}_3)(\mu_3\text{-OH})_6]OH\}_n$ (Ln = Gd, Tb, Dy)	3 D	HCl (0.1 M), NaOH (20 M)	NG	6, 72	12
PCN-601	3 D	HCl(0.1 mM), NaOH (20 M)	RT, 100	24	15
PCN-222(Fe)	3 D	HCl (12M)	NG	24	14
ZIF-8	3 D	NaOH (8 M)	100	24	15
PCN-223	3 D	HCl (1 M), pH (10)	NG	24	16

|					
[EuCd$_2$(Pbc)$_4$(Meimdc)(H$_2$O)]·3H$_2$O	3 D	pH (2-11)	NG	48	17
HZIF-1Mo	3 D	pH (1-14)	NG	168	18
[Tb(pddb)phen(ox)$_{0.5}$]$_n$	3 D	pH（4-11）	NG	120	19
HENU-1	3 D	pH (1-12)	NG	24	20
JLU-MOF58	3 D	pH (1-9)	NG	72	21
SCNU-Z1-Cl	3 D	pH (4-10)	NG	30	22
{[Zn$_2$(XN)$_2$(IPA)$_2$]·2H$_2$O}$_n$	3 D	pH (1-14)	NG	6	23
(H$_3$O)[Zn$_3$(OH)(4-cpz)$_3$]·2(DEF)·H$_2$O	3 D	pH (1-3, 12-14)	NG	24	24
[Zn(L)(H$_2$O)]·H$_2$O	3 D	pH (2-11)	NG	24	25

NG: Not Given; H$_3$L^n = (1,2-bis-(benzo[d]imidazol-2-yl)-ethenol (Ref. 2); TMA = Tetramethylammonium; H$_2$L = 2,6-bis[3-(pyrazin-2-yl)-1,2,4-triazoly] pyridine (Ref. 6); Htpbpc = 4′-[4,2′;6′,4″]-terpyridin-4′-yl-biphenyl-4-carboxylic acid; L = butanedioate (Ref. 8), TPA = 6-(1H-1,2,4-triazol-1-yl)pyridine-2-carboxylate; H$_2$ATDC = 2′-amino-1,1′:4′,1″-terphenyl- 4,4″-dicarboxylate; H$_2$L = 6,6-dimethyl-3-oxabicyclo[3.1.0]hexane-2,4-dione (Ref. 10); BPEA = 9,10-bis(pyridin-4-ylethynyl)-anthracen; HPbc = 4-(4-pyridinyl)benzoic acid; H$_3$Meimdc = 2-methyl-1H-4,5-imidazole-dicarboxylic acid; H$_2$pddb = 4,4′-(pyridine-2,6-diyl)-dibenzoic acid; phen = 1,10-phenanthroline; ox = oxalate; XN = 4'-(4-pyridine)4,2':2',4''-terpyridine; IPA = isophthalic acid, 4-cpz = 4-carboxypyrazole; H$_2$L = 5-(2-methylpyridin-4-yl)isophthalic acid (Ref. 25).

Computational details of 1 and 2

For the large molecular structures of complexes **1** and **2**, we simplified them on the basis of X-ray determined geometry but didn't perform geometry optimization (Fig. S29). Considering the symmetries of **1** and **2**, we only need to calculate two types of **Dy1** and **Dy2** fragments shown in Figure S33 for each of them. Complete-active-space self-consistent field (CASSCF) calculations on the two types of individual Dy^{III} fragments for each complex have been carried out with MOLCAS 8.4[26] program package. Each individual Dy^{III} fragment was calculated keeping the experimentally determined structure of the corresponding compound while replacing the nearest neighboring Dy^{III} ions by diamagnetic Lu^{III}.

The basis sets for all atoms are atomic natural orbitals from the MOLCAS ANO-RCC library: ANO-RCC-VTZP for Dy^{III}; VTZ for close N and O; VDZ for distant atoms. The calculations employed the second order Douglas-Kroll-Hess Hamiltonian, where scalar relativistic contractions were taken into account in the basis set and the spin-orbit couplings were handled separately in the restricted active

space state interaction (RASSI-SO) procedure. For individual Dy^{III} fragment, active electrons in 7 active orbitals include all f electrons (CAS(9 in 7 for Dy^{III})) in the CASSCF calculation. To exclude all the doubts, we calculated all the roots in the active space. We have mixed the maximum number of spin-free state which was possible with our hardware (all from 21 sextets, 128 from 224 quadruplets, 130 from 490 doublets for Dy^{III}. SINGLE_ANISO[27-29] program was used to obtain the energy levels, g tensors, magnetic axes, et $al.$ based on the above CASSCF/RASSI-SO calculations.

1_Dy1   **1_Dy2**

2_Dy1   **2_Dy2**
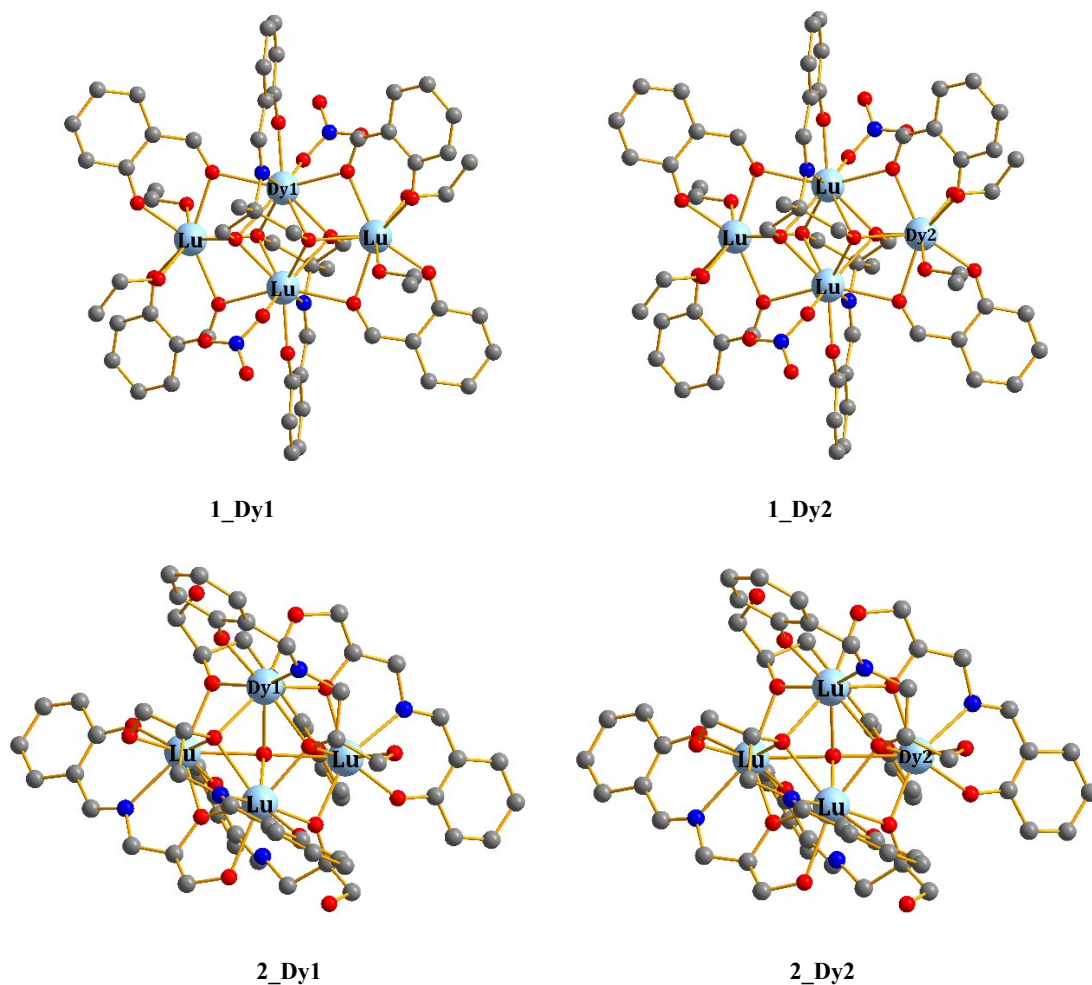
Fig. S29. Calculated model structures of individual Dy^{III} fragments in complexes **1** and **2**; H atoms are omitted for clarify.

Table S8. Calculated energy levels (cm^{-1}), g (g_x, g_y, g_z) tensors and predominant m_J values of the lowest eight Kramers doublets (KDs) of individual Dy^{III} fragments for complexes **1** and **2** using CASSCF/RASSI-SO with MOLCAS 8.4.

KDs	1_Dy1	1_Dy2

	E/cm^{-1}	g	m_J	E/cm^{-1}	g	m_J
1	0.0	0.001 0.002 19.850	±15/2	0.0	0.637 2.630 16.736	±15/2
2	194.7	0.069 0.087 17.732	±13/2	39.5	0.255 2.045 12.904	±9/2
3	291.2	0.551 0.666 13.961	±11/2	109.7	2.668 4.706 9.950	±11/2
4	368.2	4.496 5.399 10.561	±9/2	183.1	3.588 4.634 8.704	±7/2
5	417.2	0.159 2.656 10.623	±5/2	259.5	0.216 1.816 12.453	±3/2
6	495.0	0.811 2.540 13.405	±7/2	339.1	0.639 1.060 15.639	±5/2
7	573.8	0.846 1.022 15.476	±3/2	410.2	0.120 0.190 17.932	±1/2
8	641.1	0.215 0.663 18.641	±1/2	518.2	0.003 0.013 19.155	±13/2
KDs	**2_Dy1**			**2_Dy2**		
	E/cm^{-1}	g	m_J	E/cm^{-1}	g	m_J

1	0.0	0.010 0.011 19.754	±15/2	0.0	0.154 0.380 18.953	±15/2
2	124.9	0.114 0.159 16.959	±13/2	112.4	1.808 3.889 13.642	±13/2
3	250.9	0.577 0.923 13.254	±11/2	189.2	0.108 4.452 9.315	±11/2
4	341.2	0.346 0.848 9.982	±9/2	319.6	3.988 5.691 8.858	±9/2
5	401.5	2.637 6.052 9.821	±7/2	453.2	1.186 1.494 12.039	±3/2
6	490.7	2.109 4.015 8.435	±5/2	602.8	0.006 0.209 15.102	±5/2
7	544.7	1.961 6.552 12.289	±1/2	735.7	0.042 0.173 17.582	±7/2
8	685.6	0.007 0.026 19.223	±3/2	790.8	0.074 0.212 18.985	±1/2

Table S9. Wave functions with definite projection of the total moment | m_J > for the lowest two KDs of individual Dy^{III} fragments for complexes **1** and **2**.

	E/cm^{-1}	wave functions
1_Dy1	0.0	99.6%|±15/2>
	80.3	75.9%|±13/2>+18.0%|±11/2>+5.1%|±9/2>
1_Dy2	0.0	67.8%|±15/2>+13.1%|±11/2>+4.2%|±13/2>+4.0%|±3/2>+2.9%|±5/2>
	116.6	24.1%|±13/2>+20.7%|±1/2>+14.6%|±3/2>+13.9%|±5/2>+9.5%|±9/2>+8.8%|±7/2>
2_Dy1	0.0	97.8%|±15/2>
	124.9	87.0%|±13/2>+8.0%|±11/2>
2_Dy2	0.0	87.9%|±15/2>+9.2%|±11/2>
	138.8	33%|±13/2>+16.4%|±1/2>+14.1%|±9/2>+13.7%|±5/2>+13%|±3/2>+6.3%|±7/2>

1_Dy1

1_Dy2

2_Dy1

2_Dy2
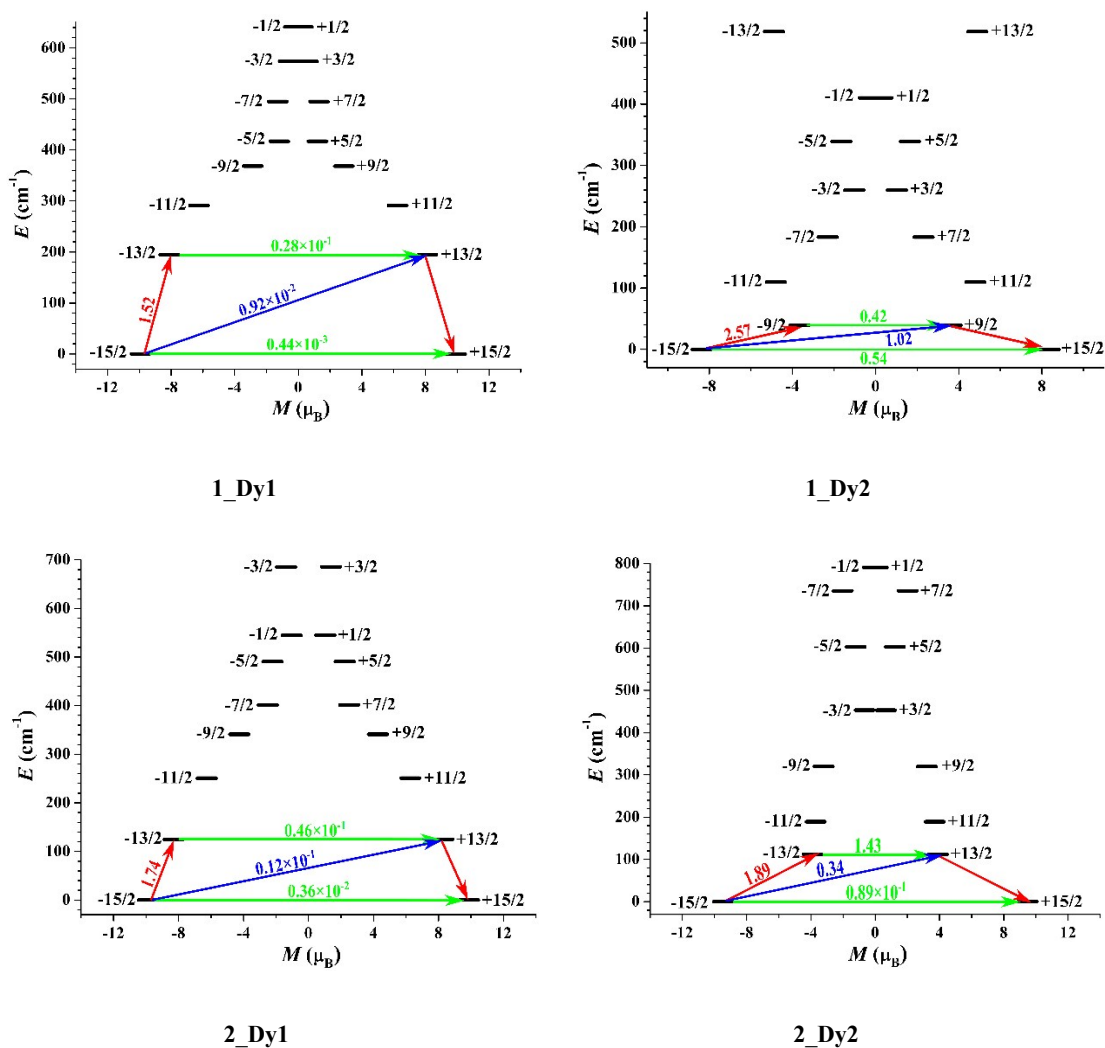
**Fig. S30**. Magnetization blocking barriers of individual Dy^{III} fragments in complexes **1** and **2**. The thick black lines represent the KDs as a function of their magnetic moment along the magnetic axis. The

green lines correspond to diagonal quantum tunneling of magnetization (QTM); the blue line represent off-diagonal relaxation process. The path shown by the red arrows represents the most probable path for magnetic relaxation in the corresponding compounds. The numbers at each arrow stand for the mean absolute value of the corresponding matrix element of transition magnetic moment.

To fit the exchange interactions between Dy^{III} ions in complexes **1** and **2**, we took two steps to obtain them. Firstly, we calculated individual Dy^{III} fragments using CASSCF/RASSI-SO to obtain the corresponding magnetic properties. Then, the exchange interactions between the magnetic centers were considered within the Lines model,[30] while the account of the dipole-dipole magnetic couplings were treated exactly. The Lines model is effective and has been successfully used widely in the research field of *d* and *f*-elements single-molecule magnets.[31,32]

For complexes **1** and **2**, there are three types of $\mathcal{J}$.
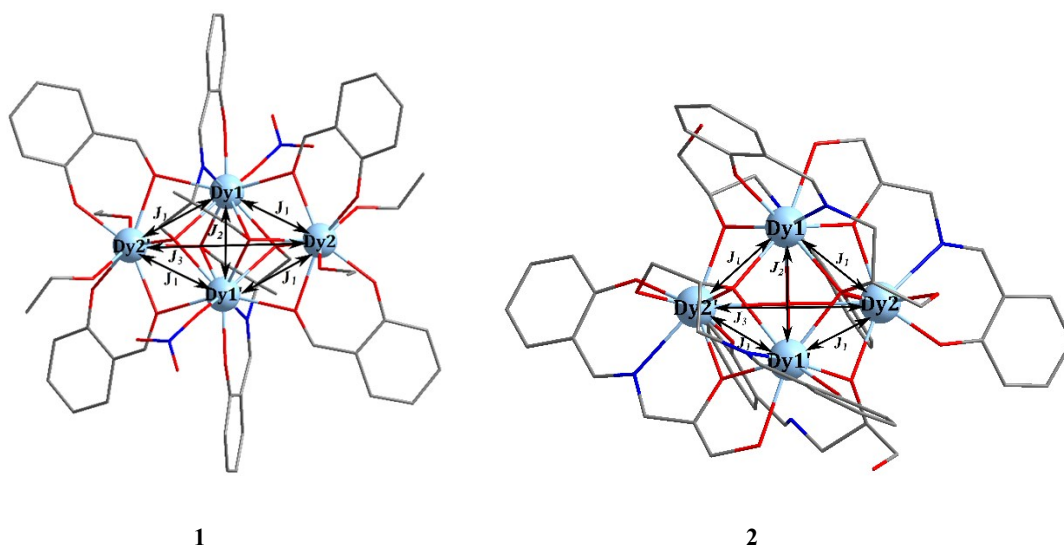
Fig. S31. Scheme of the Dy^{III}-Dy^{III} interactions in complexes **1** and **2**.

The Ising exchange Hamiltonian for **1** and **2** is:

$$H_{exch} = -J_1 \tilde{S}_{Dy1} \tilde{S}_{Dy2} - J_2 \tilde{S}_{Dy1} \tilde{S}_{Dy1'} - J_3 \tilde{S}_{Dy2} \tilde{S}_{Dy2'} \qquad (1)$$

The $\tilde{J}_1 = 25\cos\varphi J_1$, where φ is the angle between the anisotropy axes on sites Dy1 and Dy2, and J_1 is the Lines exchange coupling parameter. The other two interactions $\tilde{J}_2$ and $\tilde{J}_3$ also have similar expressions. The $\tilde{S}_{Dy} = 1/2$ is the ground pseudospin on the Dy^{III} site. The total $\tilde{J}_{total}$ is the parameter of

the total magnetic interaction $(\tilde{J}_{total} = \tilde{J}_{dipolar} + \tilde{J}_{exchange})$ between magnetic center ions. The dipolar magnetic couplings can be calculated exactly, while the Lines exchange coupling constants were fitted through comparison of the computed and measured magnetic susceptibilities using the POLY_ANISO program.[27-29]

Table S10. Exchange energies E (cm^{-1}), the energy difference between each exchange doublets Δ_t (cm^{-1}) and the main values of the g_z for the lowest four exchange doublets of complexes **1** and **2**.

	1			2		
	E	Δ_t	g_z	E	Δ_t	g_z
1	0.0	0.2×10^{-10}	20.607	0.0	0.1×10^{-8}	39.472
2	1.3	0.1×10^{-9}	39.515	1.7	0.1×10^{-8}	39.484
3	3.5	0.3×10^{-8}	39.503	2.4	0.3×10^{-9}	26.892
4	3.7	0.3×10^{-8}	0.704	6.7	0.3×10^{-7}	0.074

1 **2**
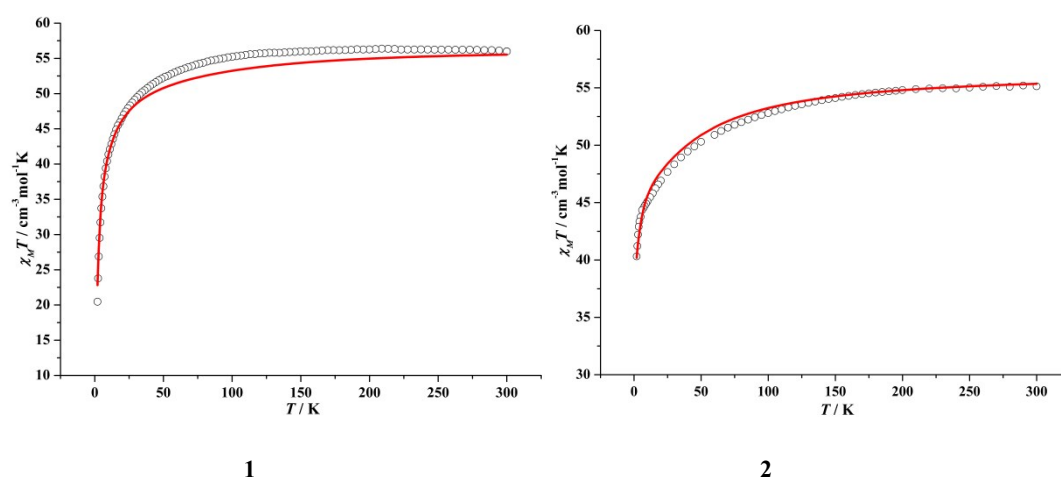
Fig. S32. Calculated (red solid line) and experimental (white circle) data of magnetic susceptibilities of complexes **1** and **2**. The intermolecular interactions zJ' of complexes **1** and **2** were fitted to −0.03 and −0.01 cm^{-1}, respectively.

1   **2**
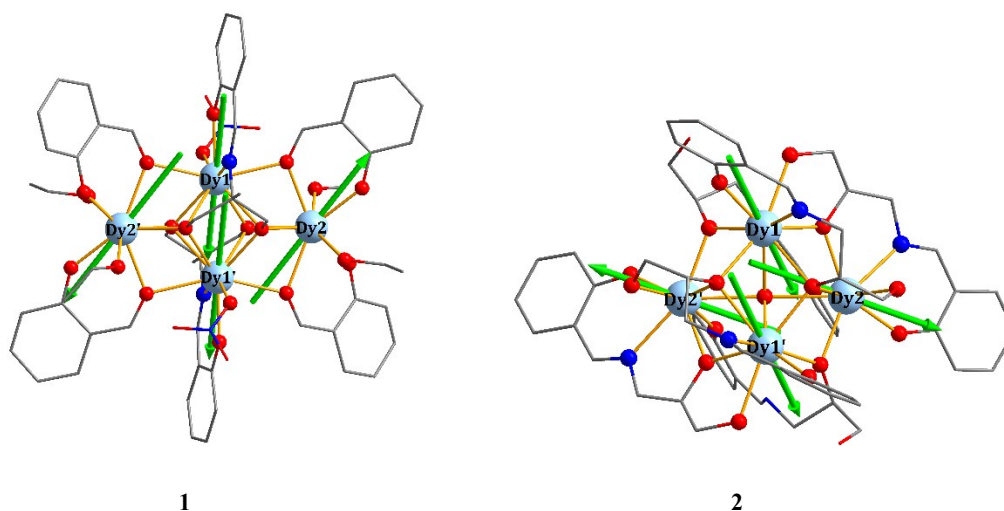
Fig. S33. Calculated orientations of the local main magnetic axes on Dy^{III} ions of complexes **1** and **2** in the ground KDs.

References

[1] X. M. Kang, H.-S. Hu, Z.-L. Wu, J.-Q. Wang, P. Cheng, J. Li, B. Zhao, *Angew. Chem. Int. Ed.*, 2019, **58**, 16610-16616.

[2] M. H. Zeng, Z. Yin, Z. H. Liu, H. B. Xu, Y.-C. Feng, Y. Hu, X.-C. Chang, Y.-X Zhang, J. Huang, and M. Kurmoo, *Angew. Chem. Int. Ed.*, 2016, **55**, 11407-11411.

[3] X. Fan, H. Fu, M.-Y. Gao, L. Zhang, and J. Zhang, *Inorg. Chem.,* 2019, 58, 13353-13359.

[4] J. H. Son and W. H. Casey, *Chem. Eur. J.*, 2016, **22**, 14155-14157.

[5] H. Fei, C. S. Han, and S. R. J. Oliver, *Inorg. Chem.*, 2012, **51**, 8655-8657.

[6] Y. Han, H. Zheng, H. Li, H. Wang, S. M. Wang, Y. Geng, and L. Wang, *RSC Adv.*, 2017, **7**, 5578-5582.

[7] J. Liu, G. Ji, J. Xiao, and Z. Liu, *Inorg. Chem.*, 2017, **56**, 4197-4205.

[8] J.-L. Shi, P. Xu, X.-G. Wang, B. Ding, X. J. Zhao, and E. C. Yang, *Z. Anorg. Allg. Chem.*, 2018, **644**, 1598-1606.

[9] J. S. Hu, S.-J. Dong, K. Wu, X. L. Zhang, J. Jiang, J. Yuan, and M. D. Zheng, *Sens. Actuators B Chem.*, 2019, **283**, 255-261.

[10] W. Qiao, T. Song, and B. Zhao, *Chin. J. Chem.*, 2019, **37**, 474-478.

[11] D. M. Chen, C. X. Sun, C. S. Liu, and M. Du, *Inorg. Chem.*, 2018, **57**, 7975-7981.

[12] J. Dong, P. Cui, P. F. Shi, P. Cheng, and B. Zhao, *J. Am. Chem. Soc.,* 2015, **137**, 15988-15991.

[13] K. Wang, X. L. Lv, D. Feng, J. Li, S. Chen, J. Sun, L. Song, Y. Xie, J. R. Li, and H. C. Zhou, *J. Am.*

Chem. Soc., 2016, **138**, 914-919.

[14] D. Feng, Z.-Y. Gu, J. R. Li, H.-L. Jiang, Z. Wei, and H. C. Zhou, *Angew. Chem. Int. Ed.,* 2012, **51**, 10307-10310.

[15] K. S. Park, Z. Ni, A. P. Côté, J. Y. Choi, R. Huang, F. J. Uribe-Romo, H. K. Chae, M. O′Keeffe, and O. M. Yaghi, *Proc. Natl. Acad. Sci. U. S. A.* 2006, **103**, 10186-10191.

[16] D. Feng, Z. Y. Gu, Y.-P. Chen, J. Park, Z. Wei, Y. Sun, M. Bosch, S. Yuan, and H. C. Zhou, *J. Am. Chem. Soc.*, 2014, **136**, 17714-17717.

[17] L. Ding, L. H. Liu, Q. Shi, Y. Q. Sun, Y. J. Wang, and Y. P. Chen, *Inorg. Chem.*, 2017, **56**, 14850-14858.

[18] Y. Wang, F. Wang, and J. Zhang, *Cryst. Growth Des.*, 2019, **19**, 3430-3434.

[19] X. L. Qu and B. Yan, *Inorg. Chem.*, 2019, **58**, 524-534.

[20] D. Li, Q. Xu, Y. Li, Y. Qiu, P. Ma, J. Niu, and J. Wang, *Inorg. Chem.*, 2019, **58**, 4945-4953.

[21] X. Sun, J. Gu, Y. Yuan, C. Yu, J. Li, H. Shan, G. Li, and Y. Liu, *Inorg. Chem.*, 2019, **58**, 7480-7487.

[22] S. Q. Deng, X. J. Mo, S. R. Zheng, X. Jin, Y. Gao, S. L. Cai, J. Fan, and W. G. Zhang, *Inorg. Chem.*, 2019, **58**, 2899-2909.

[23] X.-M. Kang, X. Y. Fan, P. Y. Hao, W. M. Wang, and B. Zhao, *Inorg. Chem. Front.*, 2019, **6**, 271-277.

[24] H.-R. Fu, F. Wang, and J. Zhang, *Dalton Trans.*, 2015, **44**, 2893-2896.

[25] X. Y. Guo, F. Zhao, J. J. Liu, Z. L. Liu, and Y. Q. Wang, *J. Mater. Chem. A*, 2017, **5**, 20035-20043.

[26] F. Aquilante, J. Autschbach, R. K. Carlson, L. F. Chibotaru, M. G. Delcey, L. De Vico, I. Fdez. Galván, N. Ferré, L. M. Frutos, L. Gagliardi, M. Garavelli, A. Giussani, C. E. Hoyer, G. Li Manni, H. Lischka, D. Ma, P. Å. Malmqvist, T. Müller, A. Nenov, M. Olivucci, T. B. Pedersen, D. Peng, F. Plasser, B. Pritchard, M. Reiher, I. Rivalta, I. Schapiro, J. Segarra-Martí, M. Stenrup, D. G. Truhlar, L. Ungur, A. Valentini, S. Vancoillie, V. Veryazov, V. P. Vysotskiy, O. Weingart, F. Zapata, R. Lindh, *J. Comput. Chem.*, 2016, **37**, 506-541.

[27] L. F. Chibotaru, L. Ungur, A. Soncini, *Angew. Chem. Int. Ed.*, 2008, **47**, 4126-4129.

[28] L. Ungur, W. Van den Heuvel, L. F. Chibotaru, *New J. Chem.*, 2009, **33**, 1224-1230.

[29] L. F. Chibotaru, L. Ungur, C. Aronica, H. Elmoll, G. Pilet, D. Luneau, *J. Am. Chem. Soc.*, 2008, **130**, 12445-12455.

[30] M. E. Lines, *J. Chem. Phys.*, 1971, **55**, 2977-2984.

[31] K. C. Mondal, A. Sundt, Y. H. Lan, G. E. Kostakis, O. Waldmann, L. Ungur, L. F. Chibotaru, C. E. Anson, A. K. Powell, *Angew. Chem. Int. Ed.*, 2012, **51**, 7550-7554.

[32] S. K. Langley, D. P. Wielechowski, V. Vieru, N. F. Chilton, B. Moubaraki, B. F. Abrahams, L. F. Chibotaru, K. S. Murray, *Angew. Chem. Int. Ed.*, 2013, **52**, 12014-12019.